

Summary Report for FIRE Spectrometer HgCdTe Detector Array

Craig W. McMurtry, Judith L. Pipher and William J. Forrest

University of Rochester, Rochester, NY, USA

ABSTRACT

This is a summary report covering the tests and data obtained by University of Rochester during the validation of the HAWAII-2RG FIRE-1 HgCdTe detector array. The infrared detector array was purchased from Teledyne Imaging Sensors (TIS), and will be used as the primary detector array in the FIRE spectrometer, which is a facility class instrument for the Magellan Telescopes.

Keywords: HgCdTe, HAWAII-2RG, Teledyne, infrared, dark current, noise, quantum efficiency

1. INTRODUCTION

Unless otherwise stated, all tests were performed with the FIRE-1 detector array operating at $T=77.5\text{K}$ with an applied detector reverse bias of 250mV. Because of an undiagnosed noise problem with the University of Rochester's 4-channel array controller electronics, we had to use our 2-channel array controller. We continued to take data using the HAWAII-2RG in 4 output mode (i.e. outputs 7, 15, 23, 31). Since we had to run every test for the first two outputs and then the third and fourth outputs, this required twice as much time to complete all tests.

2. DATA

2.1. Clocks and Biases

Operating parameters (clocks and biases) are provided in Table 1. Test procedures are detailed by Wu et al.¹

2.2. Laboratory Calibration

We measured the source follower gain of the ROIC to be 0.9296 (see Figure 1).

The conversion gain for the UR system is $1.929e^-/ADU$ as measured using the noise squared versus signal method (see Figure 2). This conversion gain corresponds to a nodal capacitance of 45.43 fF.

We determined the non-linearity correction to the output signal as a function of detector de-biasing (see Figure 3). For the applied detector reverse bias of 250 mV, the actual well depth is 129,850 e^- or 457.9 mV input referred. With the non-linearity correction applied, the well depth is 142,690 e^- or 503.2 mV input referred.

Following the autocorrelation methods outlined by Moore *et al.*,^{2,3} we measured the interpixel capacitive coupling to be 7.8%. The interpixel capacitance (IPC) correction will **NOT** be applied to data through-out this report, but will instead be applied as a separate column in the final summary (see Table 3).

Table 1. Voltages used for clocks and biases with SCA FIRE-1 operating at T=77.5K.

Clock	Value (Volts)
ϕ FSyncB	0.0 / 3.3
ϕ VClk	0.0 / 3.3
ϕ LSyncB	0.0 / 3.3
ϕ HClk	0.0 / 3.3
ϕ ResetEn	0.0 / 3.3
ϕ ReadEn	0.0 / 3.3
ϕ CSB	0.0 / 3.3
ϕ MainResetB	0.0 / 3.3

Bias	Value (Volts)
Vdd	3.3
Vdda	3.3
CellDrain	0.0
Drain	0.0
Vbiaspower	3.3
Vbiasgate	2.4
Vload	3.3
Vreset	0.10
Dsub	0.35*

* The applied detector reverse bias was 250mV, i.e. Vreset - Dsub.

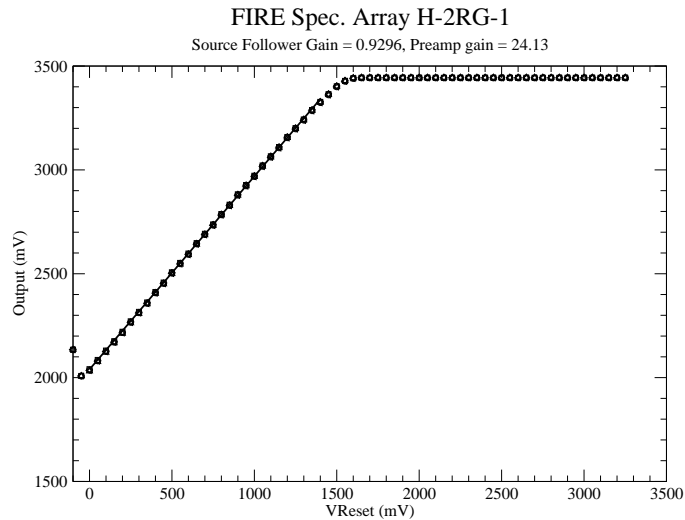


Figure 1. This graph shows the output voltage versus input voltage, where the slope is the Source Follower gain of the ROIC's signal path.

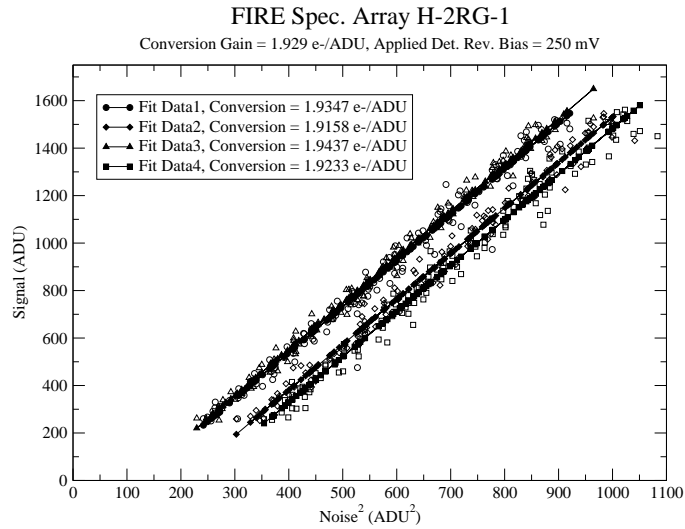


Figure 2. This graph shows the signal versus noise squared, where the slope is the conversion gain (or transimpedance gain) at the given applied detector reverse bias. Notice that the data were obtained at relatively low signal levels to avoid the need for non-linearity corrections.

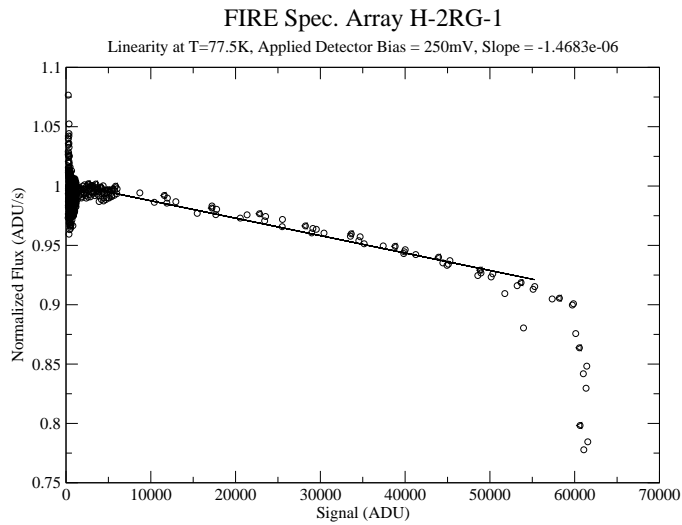


Figure 3. This graph shows the normalized flux versus signal. For a linear device the normalized flux versus signal should have a flat response at 1. Since the capacitance of the detector diodes changes as they integrate charge (i.e. de-bias), there is an inherent non-linearity, which reaches a maximum of about 10% at saturation for this device.

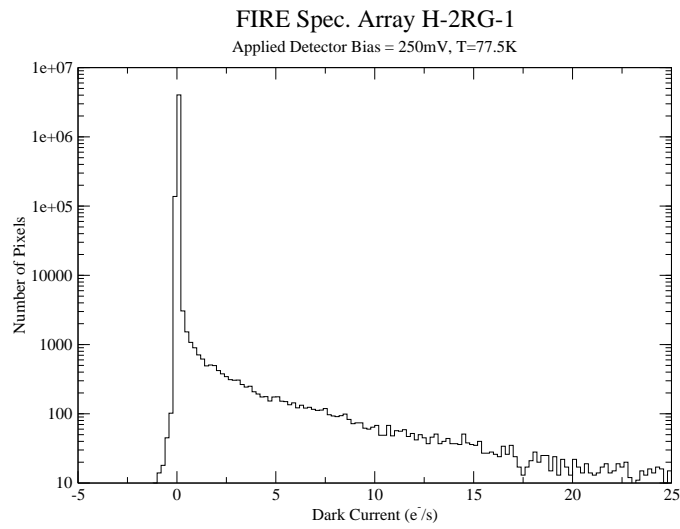


Figure 4. Histogram of dark current.

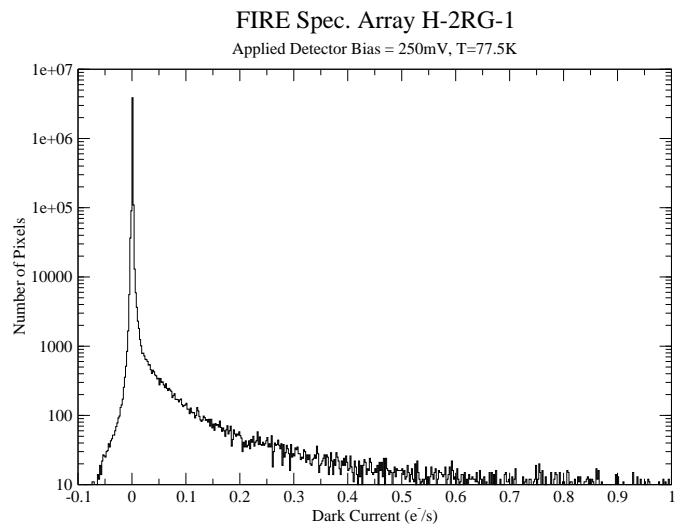


Figure 5. Histogram of dark current.

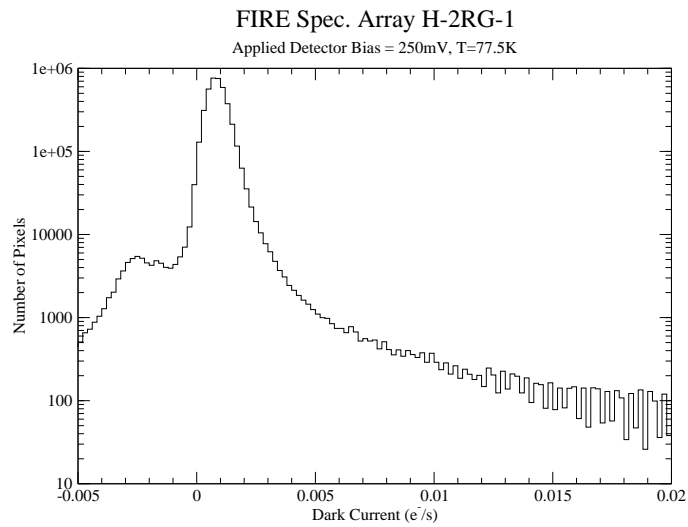


Figure 6. Histogram of dark current.

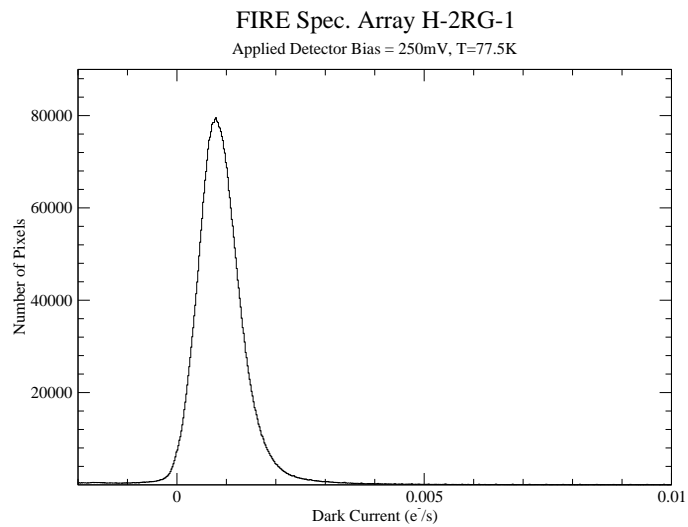


Figure 7. Histogram of dark current. The median dark current is $0.00085e^-/s$.

2.3. Dark Current

We measured the dark current for the FIRE-1 SCA at an applied detector reverse bias of 250mV (see Figures 4 to 7). Please note that there is substantially less high dark current tail in this HgCdTe detector array as compared with older generation (NICMOS3) HgCdTe detector arrays. In fact, the distribution (but not magnitude) of dark current in this HgCdTe detector array is very similar to what has been obtained for InSb detector arrays, where the distribution is almost Gaussian (although with a mean value higher due to its longer wavelength response). TIS's near elimination of the high dark current tail in 2.5 μ m cutoff HgCdTe detector arrays is a great achievement, which positively impacts the operability.

We employed a darkened cold baffle around the FPA. In the past, with proper, cold, dark baffles we have achieved light leaks $< 0.002e^-/s$ for InSb SCAs, which is dominated by contribution at the longer wavelengths (3 to 5.4 μ m). We expect that the light leak levels are $< 0.0002e^-/s$ (factor of ten lower) for a detector array with a cut-off wavelength of 2.5 μ m. Therefore we are confident that the dark current is not limited by a light leak.

We first measured the dark current on the left half of the array (outputs 7 & 15). Since the test report from TIS indicated that the dark current is $0.004 \pm 0.004e^-/s$, we thought that SUTR integrations lasting about 20,000 seconds would be sufficiently long enough to determine the accumulated dark charge over time with the given read noise. With a 2000 SUTR at 11.1 seconds frame read time (22,200 seconds integration), we obtained a dark current value of $0.001 \pm 0.001e^-/s/pixel$, i.e. approximately $22e^-$ dark charge with a CDS noise of $22e^-$ for a S/N = 1. Unfortunately, we needed to integrate longer than 40,000 seconds just to obtain a S/N = 2 on the dark current data. We took a 4000 SUTR data set (44,400 sec integration) for the right half of the array (outputs 23 & 31). These data produced a dark current of $0.0007 \pm 0.0004e^-/s/pixel$. Although the dark current for both data sets is the same to within the uncertainties (as well as the TIS measured values), there is considerable difference in the two halves of the array as seen in Figure 8. The median dark current value for the entire detector array is $0.00085 \pm 0.001e^-/s/pixel$.

2.4. Noise

We measured the noise per pixel using the “temporal” method, i.e. numerous images taken using identical parameters (see Figures 9 to 16). We used reference pixels to correct for frame-to-frame drift, but we did not use the reference pixels to correct for row noise, which is mostly a 1/f drift (possible benefit is about $2 - 4e^-$).

There is a slight tail to higher noise present in each of the graphs. We investigated that tail to determine its origin, e.g. from cosmic ray hits that were not rejected or higher dark current. As the reader can see from Figure 17, the pixels with high noise tend to always have high noise and thus can be attributed to higher dark current or RTN.

2.4.1. Random Telegraph Noise

Random Telegraph Noise (RTN) noise is also known as random telegraph signal (RTS) or burst noise or popcorn noise, see Bacon *et al.*⁴

2.5. Quantum Efficiency

The quantum efficiency (QE) of the FIRE HgCdTe detector arrays was measured at three different wavelengths. Those results can be found in Table 3. A representative flatfield is shown in Figure 19.

2.6. Residual Images

Residual, persistent, latent or ghost images are the left-over signals in any subsequent (dark) image after exposure to a bright source (see Benson, *et al.*⁵). The original Spitzer Category III requirements on residual images are given in Table 2.

For further information, E-mail: craig.mcmurtry@rochester.edu

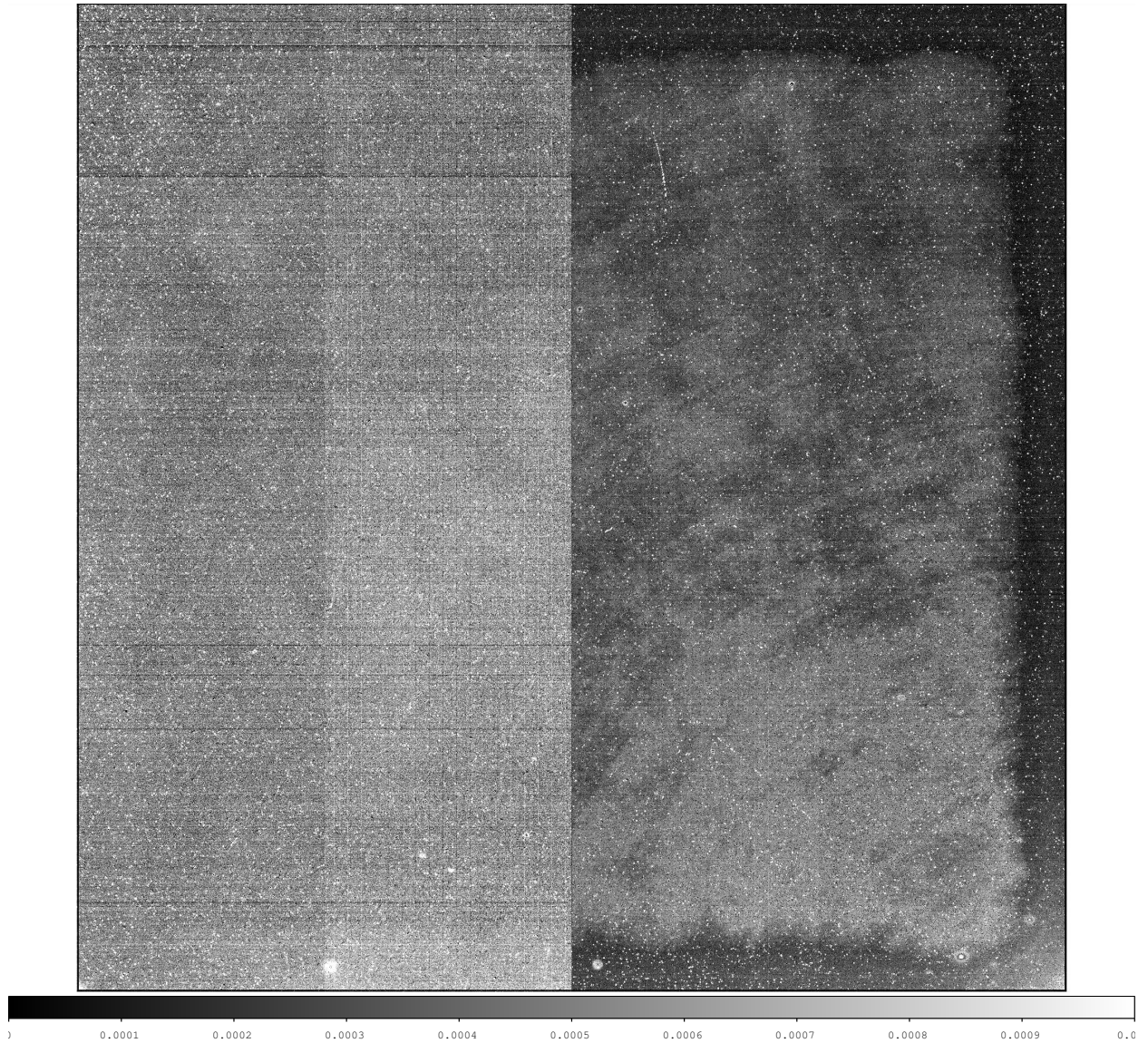


Figure 8. Image of dark current per pixel displayed on linear scaling in units of ADU/sec, where 1 ADU = 1.929 e-.

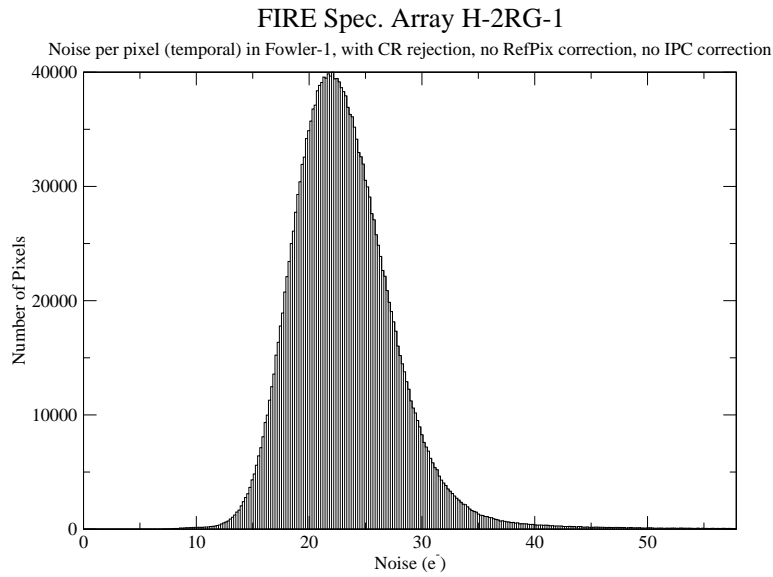


Figure 9. This graph shows a histogram of noise per pixel using Fowler-1 sample pairs, also known as Correlated-Double Sampling (CDS).

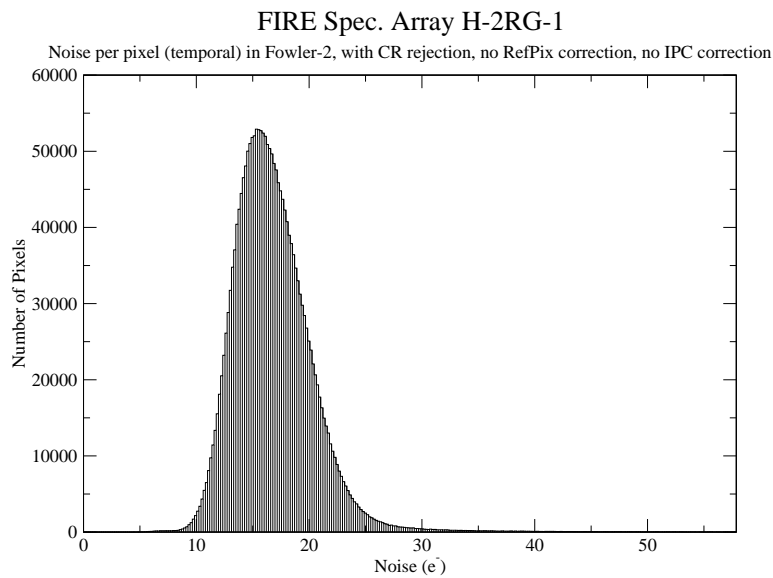


Figure 10. This graph shows a histogram of noise per pixel using Fowler-2 sample pairs.

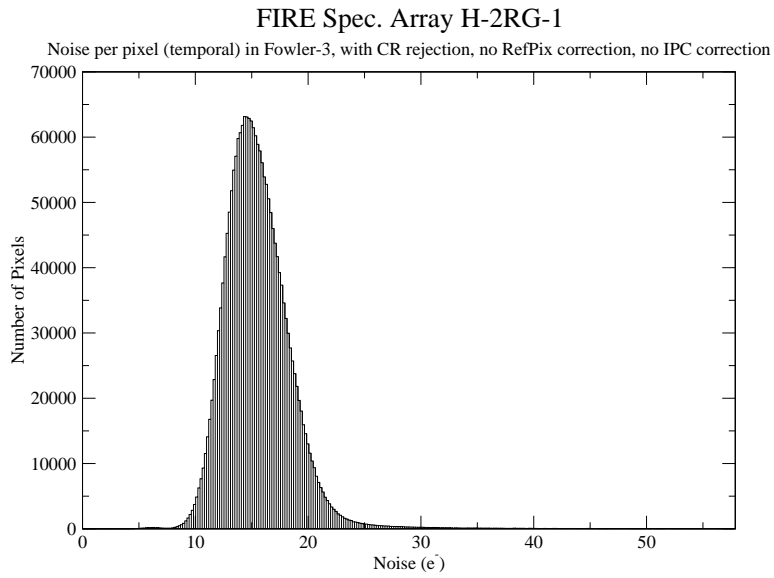


Figure 11. This graph shows a histogram of noise per pixel using Fowler-3 sample pairs.

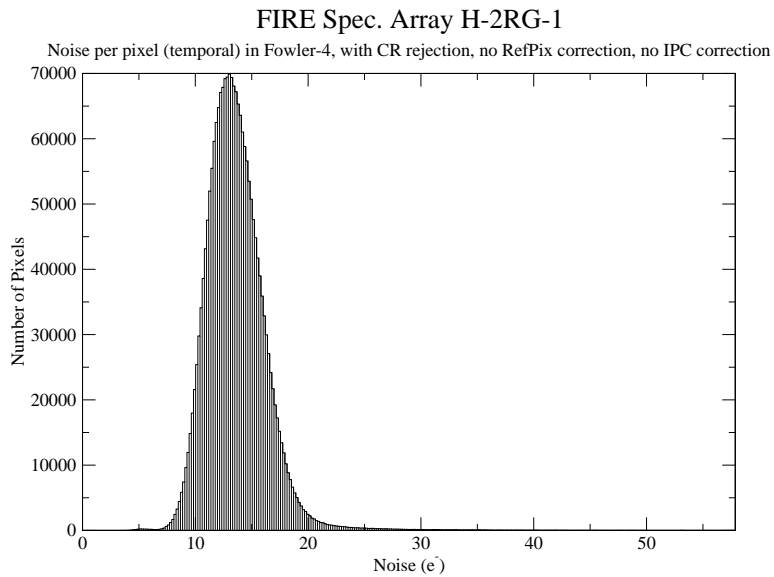


Figure 12. This graph shows a histogram of noise per pixel using Fowler-4 sample pairs.

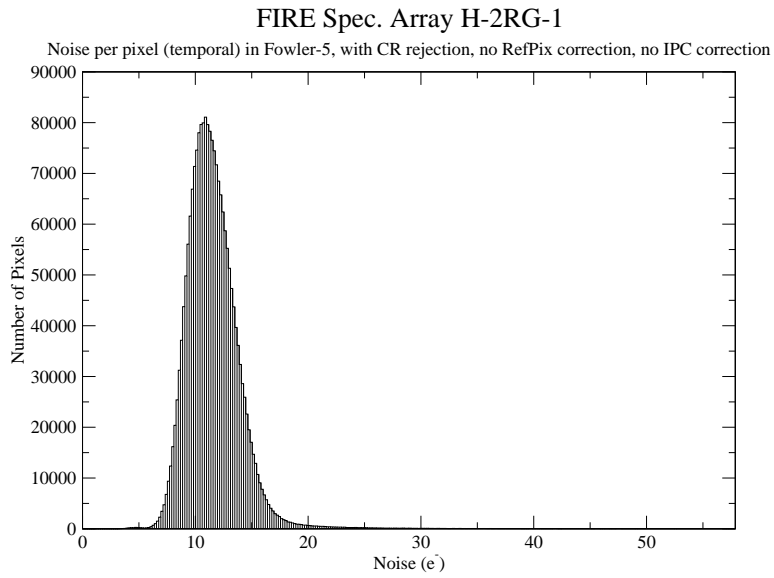


Figure 13. This graph shows a histogram of noise per pixel using Fowler-5 sample pairs.

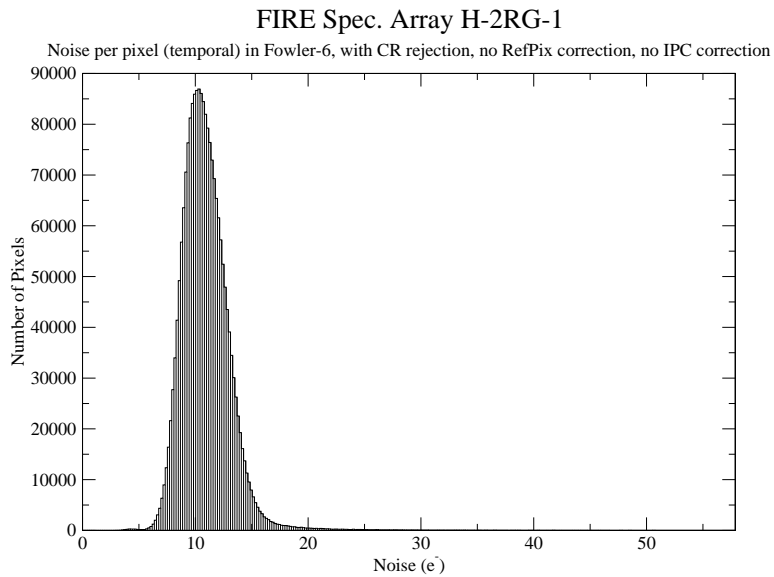


Figure 14. This graph shows a histogram of noise per pixel using Fowler-6 sample pairs.

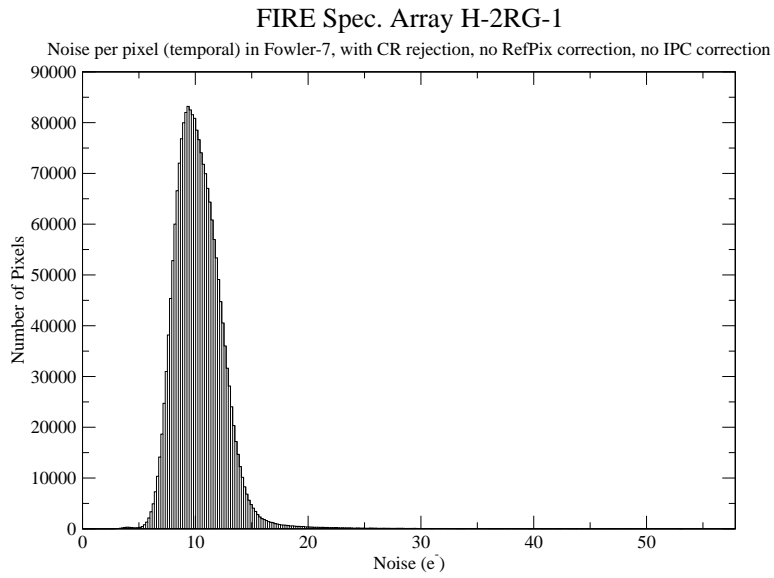


Figure 15. This graph shows a histogram of noise per pixel using Fowler-7 sample pairs.

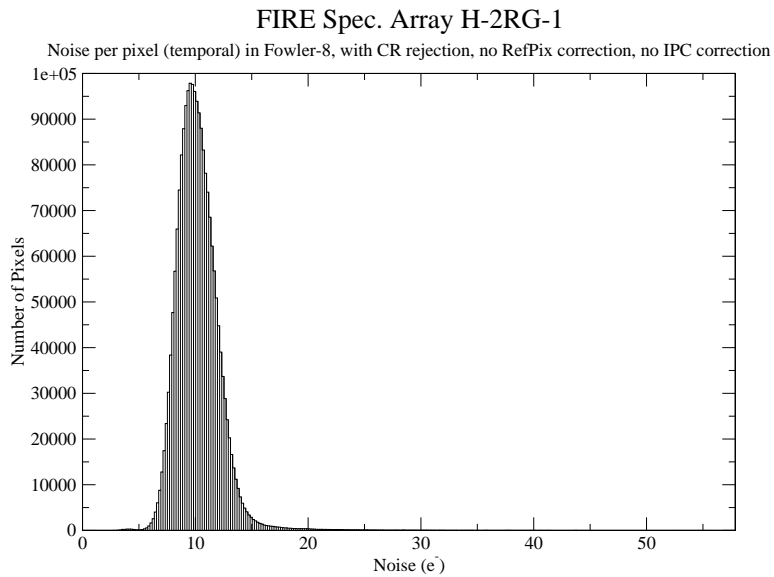


Figure 16. This graph shows a histogram of noise per pixel using Fowler-8 sample pairs.

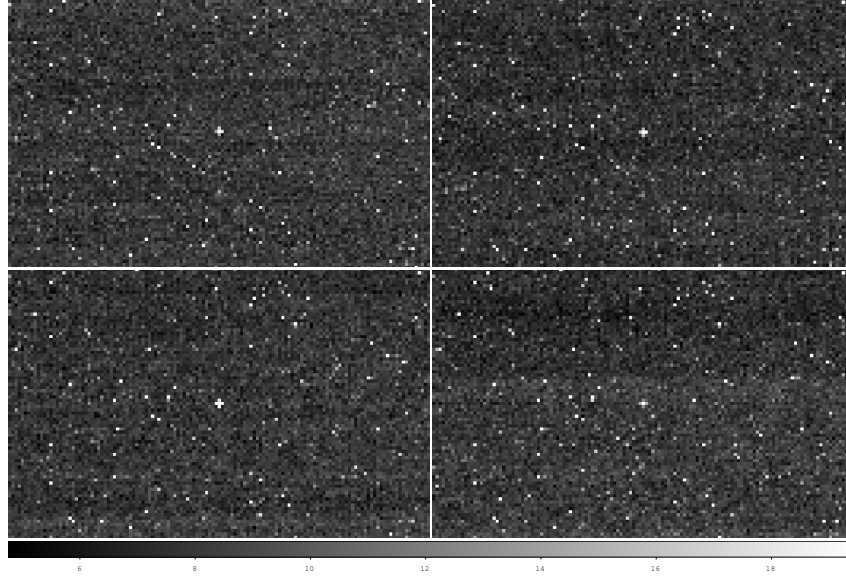


Figure 17. This figure shows the noise per pixel over a sample region in each of four separate noise maps. The images are for Fowler-1 sample pairs, Fowler-2, Fowler-8 and Fowler-4 clockwise from the upper left. The scale is from 5 to 19 ADU, where 1 ADU = 1.929 e⁻.

2.7. Operability

The basic operability is defined as the number of pixels that respond light, i.e. not dead pixels. The basic operability is > 99.7%. The total operability is defined as the percentage (or number) of pixels that are all operable in a union of the individual parameter operabilities, where the parameter operabilities are defined as the percentage of pixels that satisfy the requirement for that given parameter, e.g. QE operability or noise operability. The dark current operability is 98.509% and is shown in Figure 20. The quantum efficiency operabilities (see Figures 21-23) are 99.3086 % or 4132828 pixels for J-broadband, 99.5756 % or 4143939 pixels for H-broadband, and 99.3965 % or 4136484 pixels for K-broadband. The read noise operability is 3669320 pixels or 88.1709 % and is shown in Figure 24. The total operability is 3614013 pixels or 86.8419%, which is dominated by the read noise operability. If neglecting the read noise requirement, then the operability is 4090365 pixels or 98.2883 %.

Table 2. Image residuals per pixel requirement for Spitzer Space Telescope IRAC InSb detector arrays.

	Source Flux (e ⁻ /s)	Source Exposure (s)	Source Fluence (e ⁻)	Delay (s)	Residual Integration Time (s)	Required * Residual Fluence (e ⁻)
Residual Test 1	2500	20	50000	0	20	10
Residual Test 2	2500	20	50000	200	20	1
Residual Test 3	250	200	50000	0	200	5
Residual Test 4	2500	100	250000	0	20	100
Residual Test 5	2500	100	250000	200	20	10

* Any residual image must be below the required residual fluence (for the given integration time) after the listed delay.

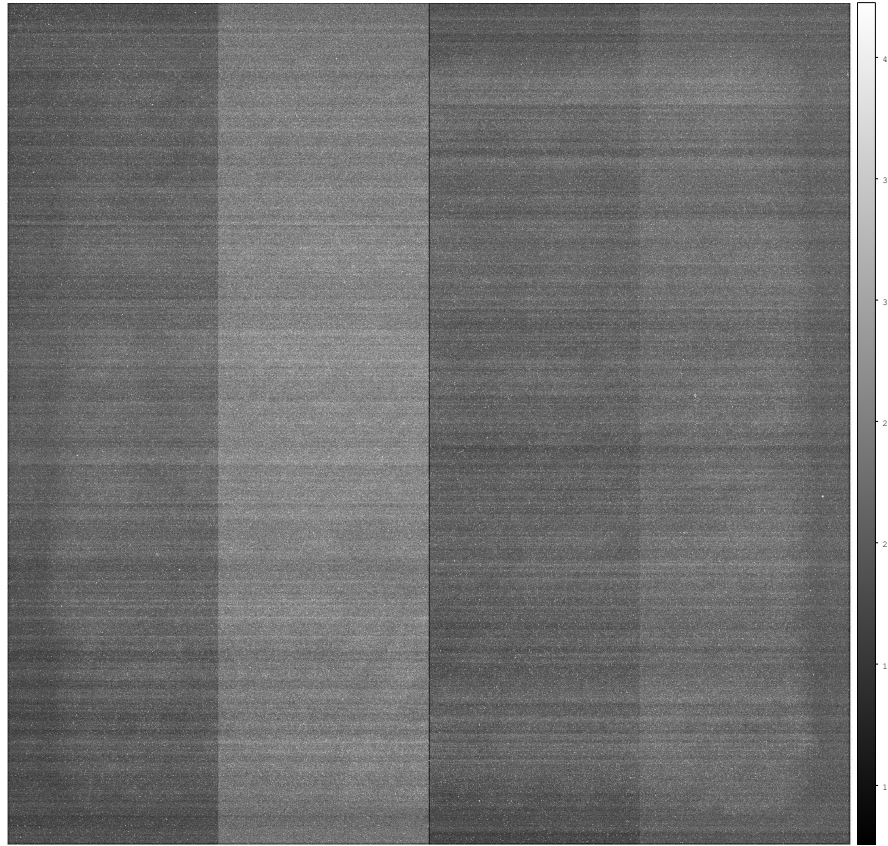


Figure 18. This figure shows the noise in electrons per pixel. The higher noise on the second output is partially (but not entirely) due to higher noise in our electronics for that channel.

3. CONCLUSIONS

The FIRE-1 detector array is an excellent device that will meet the science driven requirements of the FIRE spectrometer.

ACKNOWLEDGMENTS

Funding for this work was provided by: MIT FIRE Instrument NSF-MRI, Award No. ???, sub-contract to University of Rochester.

REFERENCES

1. J. Wu, W. J. Forrest, J. L. Pipher, N. Lum, and A. Hoffman, “Development of infrared focal plane arrays for space,” *Review of Scientific Instruments* **68**, pp. 3566–3578, 1997.
2. A. C. Moore, Z. Ninkov, and W. J. Forrest, “QE Overestimation and Deterministic Crosstalk Resulting from Inter-pixel Capacitance,” in *Optical Eng.*, 2003.
3. A. C. Moore, Z. Ninkov, and W. J. Forrest, “Interpixel Capacitance in Nondestructive Read-out Focal Plane Arrays,” in *Proc. SPIE, Focal Plane Arrays for Space Telescopes*, T. J. Grycewicz and C. R. McCreight, eds., **5167**, pp. 204–215, 2003.
4. C. M. Bacon, C. W. McMurtry, J. L. Pipher, W. J. Forrest, and J. D. Garnett, “Burst noise in the HAWAII-1RG multiplexer,” in *Proc. SPIE, Focal Plane Arrays for Space Telescopes II*, T. J. Grycewicz and C. J. Marshall, eds., **5902**, pp. K1–K12, 2005.

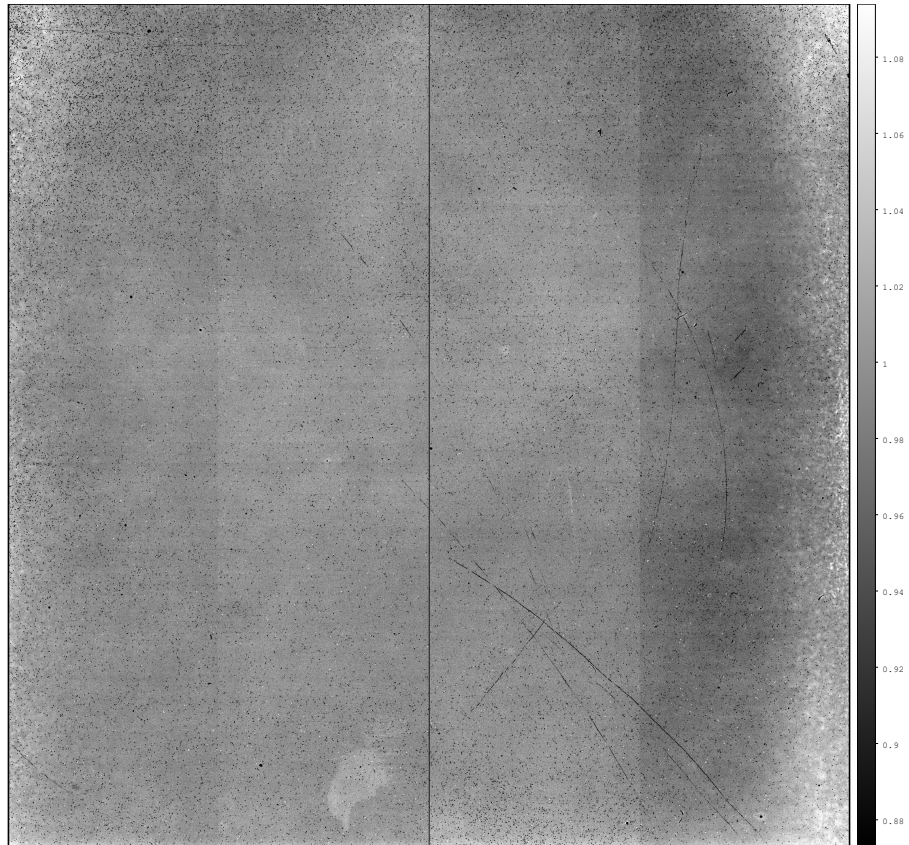


Figure 19. This figure shows flat field for the array. The data have been corrected for $\cos^4\theta$ illumination fall-off and have been normalized to the central region. The correction for $\cos^4\theta$ is slightly offset with respect to the true optical axis, as is evidenced by the light region on the right side. At the center of the array is a dark column, which is labeled as inoperable in the QE maps. This column may not be truly inoperable since it does not appear in the data taken by Teledyne.

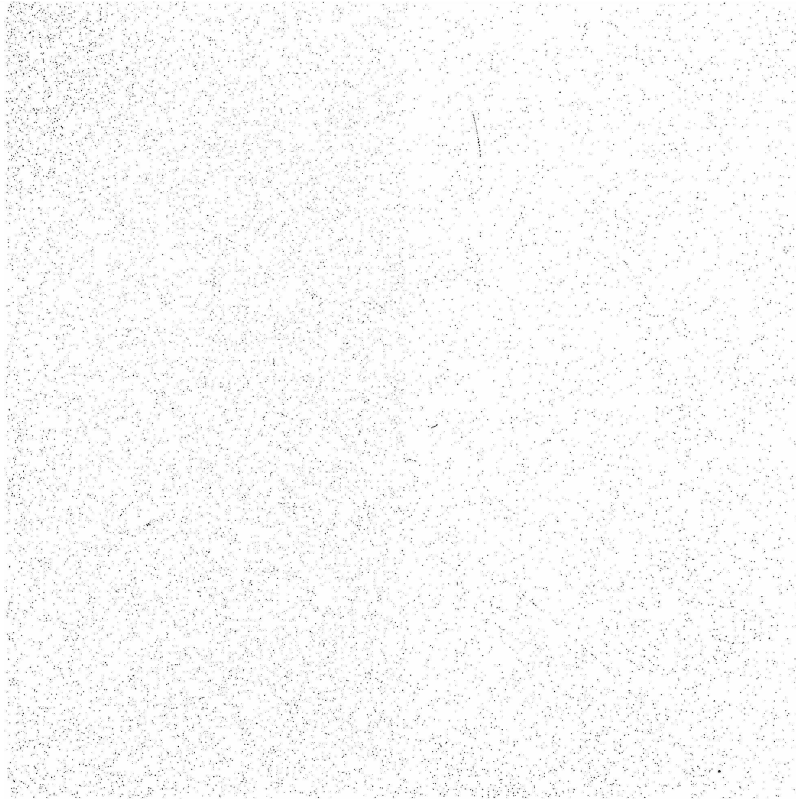


Figure 20. This figure shows the dark current operability map, where white is operable and dark is inoperable, i.e. dark current $> 0.01e^-/s$. The number of operable pixels is 4099556 or 98.509%.

5. R. G. Benson, W. J. Forrest, J. L. Pipher, W. J. Glaccum, and S. L. Solomon, "Spatial distributions of hole traps and image latency in InSb focal plane arrays," in *Proc. SPIE, Infrared Spaceborne Remote Sensing VIII*, M. Strojnik and B. F. Andresen, eds., **4131**, pp. 171–184, 2000.



Figure 21. This figure shows the quantum efficiency operability map at J-band, where white is operable and dark is inoperable. The quantum efficiency limit for operability is $> 70\%$. The number of operable pixels is 99.3086 % or 4132828.



Figure 22. This figure shows the quantum efficiency operability map at H-band, where white is operable and dark is inoperable. The quantum efficiency limit for operability is $> 70\%$. The number of operable pixels is 99.5756 % or 4143939.



Figure 23. This figure shows the quantum efficiency operability map at K-band, where white is operable and dark is inoperable. The quantum efficiency limit for operability is $> 70\%$. The number of operable pixels is 99.3965 % or 4136484.

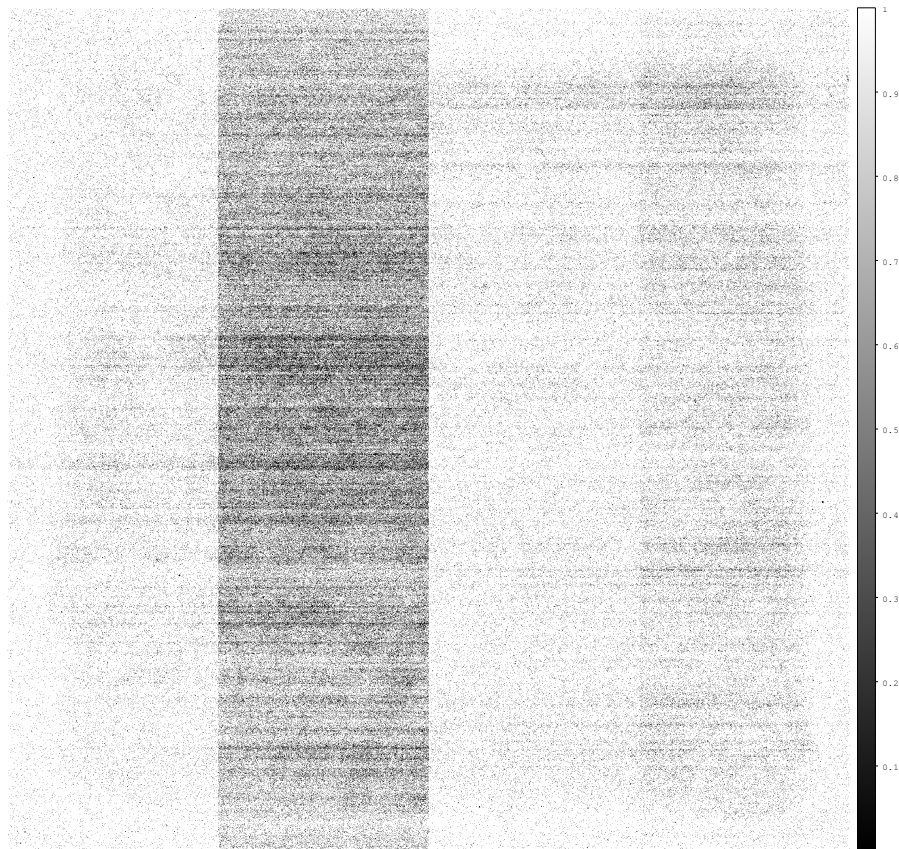


Figure 24. This figure shows the operability based upon the noise, where inoperable is defined as a noise $> 25e^-$. The higher noise on the second output is partially (but not entirely) due to higher noise in our electronics for that channel. The number of operable pixels is 3669320 or 88.1709 %.

Table 3. Summary of Performance For FIRE-1 infrared detector array. All data taken at T=77.5K with 250 mV applied detector reverse bias.

Parameter	Unit	Specification	Goal	Measured	IPC corrected	Comment
Read-out integrated circuit		HAWAII-2RG				By Design
Number of pixels		2048 × 2048				By Design
Pixel Size	μm	18				By Design
Outputs		1, 4, 32		4		more testing
Power Dissipation	mW	< 1.0	< 0.5			
Detector Material		HgCdTe				By Process
Detector Substrate		CdZnTe	removed			By Process
Cutoff wavelength	μm	2.45 - 2.65	2.50 - 2.55			
Quantum Efficiency						
(0.6 - 1.0 μm)	%	> 55	> 70			
(J 1.25 μm)	%	> 70	> 80	95	88	
(H 1.65 μm)	%	> 70	> 80	103	95	
(K 2.23 μm)	%	> 70	> 80	98	90	
Median Dark Current	e^-/s	< 0.1	< 0.01	0.0009	0.0008	
Median Read Noise (CDS)	e^-	< 25	< 15	22	20	
Noise (Fowler-8)	e^-			9.5	8.8	
Well Capacity	e^-	> 65,000	> 100,000	142,700	131,600	
Well Capacity	mV			503.2	463.9	input referred
Crosstalk	%	< 5	< 2			
Interpixel Capacitance	%	< 2	< 1.5	7.8 total	NA	all neighbors
Residual Image	%	< 0.1	< 0.01			
Operability	%	> 95	> 99		86.84 (98.29)	
Bad Pixel Clusters	%	< 1	< 0.5			
SCA Flatness	μm	< 30	< 10			
SCA Parallelism	μm	< 50	< 25			